arXiv:astro-ph/0205470 v1 27 May 2002

X-ray temporal properties of XTE J1650−500 during outburst decay

E. Kalemci[1], J. A. Tomsick[1], R. E. Rothschild[1], K. Pottschmidt[2,3,4], S. Corbel[5], R. Wijnands[6,7], J. M. Miller[6], P. Kaaret[8]

ABSTRACT

We investigated the temporal behavior of the new black hole transient XTE J1650−500 with the *Rossi X-ray Timing Explorer (RXTE)* as the source made a transition to the low/hard state during the decay of the 2001 outburst. We find QPOs in the 4 – 9 Hz range, enhanced time lags and reduced coherence during the state transition. We also observe a shift in the peak frequency of the noise component with energy during the transition. The evolution of the power spectrum as well as the lag and coherence behavior during the state transition are similar to the state transitions observed for other black hole sources, especially Cyg X-1. The temporal properties during the transition to the low state put constraints on the accretion geometry of XTE J1650−500 and may have implications for all black hole binary systems. We suggest a possible geometry and evolution of a jet+corona+disk system based on enhanced lags and peak frequency shift during the transition.

Subject headings: stars:individual (XTE J1650−500) – black hole physics – X-rays:stars

---

[1]Center for Astrophysics and Space Sciences, Code 0424, University of California at San Diego, La Jolla, CA, 92093-0424, USA

[2]Institut für Astronomie und Astrophysik, Abt. Astronomie, Sand 1, 72076 Tübingen, Germany

[3]*INTEGRAL* Science Data Center, Chemin d'Écogia 16, 1290 Versoix, Switzerland

[4]Max Planck Institut für Extraterrestische Physik, Postfach 1312, 85741 Garching, Germany

[5]Université Paris VII and Service d'Astrophysique, CEA Saclay, F-91191 Gif sur Yvette, France

[6]Center for Space Research, 70 Vassar Street, NE-80/6055, MIT, Cambridge, MA, 02139, USA

[7]Chandra Fellow

[8]Harvard-Smithsonian Center for Astrophysics, 60 Garden Street, Cambridge, CA, 02138, USA

1. Introduction

Galactic black hole candidates (BHC) exhibit transitions between X-ray states distinguished by their different spectral and timing properties (Tanaka & Lewin 1995). The classification of these states is not rigorously defined and is an active topic of debate. The accretion rate seems to be the most important parameter determining the spectral states, although it is argued by Homan et al. (2001) that two independent parameters are needed to describe the states, and the second parameter could possibly be the size of the Comptonizing region. Five states have been frequently quoted: the off state, the low-hard state (LS), the intermediate state (IS), the high-soft state (HS) and the very-high state (VHS). They are named after their spectral and luminosity properties, but also show very distinct temporal and radio properties. The HS is dominated by a soft spectrum with little or no timing noise (rms amplitude less than a few %), and the radio emission is quenched (Fender et al. 1999; Corbel et al. 2000). On the other hand, the LS is dominated by a power law component in the X-ray spectrum, which is often interpreted as being associated with a hot electron corona, and shows very strong band limited noise (up to 50% rms amplitude) and quasi-periodic-oscillations (QPO). Moreover, the radio observations often reveal a compact jet during this state (Corbel et al. 2001; Fender et al. 2001, and references therein). The IS/VHS shows both an ultra-soft spectral component and a power-law tail with 1% – 15% rms variability. Some of the BHCs show high frequency QPOs (with frequencies of several hundreds of Hz) in this state. The compact jet is also quenched in the IS/VHS, i.e. in any state where a soft, strong X-ray component exists (Corbel et al. 2001).

The geometry of the accretion system in each state and the triggering mechanism for the state transitions are not well understood (Nowak, Wilms & Dove 2002). The most notable observational properties during the transition to the LS are (1) the appearance of QPOs and strong band limited noise in the power density spectrum (PSD) and the hardening of the power law component in the X-ray spectrum, possibly indicating the formation of a hot corona, (2) the evolution of the characteristic frequencies of the power spectrum which might indicate retreating of the inner-disk radius (di Matteo & Psaltis 1999; Tomsick & Kaaret 2000; Kalemci et al. 2001), (3) optically thin synchrotron radio emission indicating plasma ejections and formation of compact radio jets (Corbel et al. 2000), and (4) a decrease in coherence and an increase in time lags observed in Cyg X-1 which might be related to the radio jets (Pottschmidt et al. 2000).

Here, we describe a state transition found in the soft X-ray transient XTE J1650−500 in light of the observations above. XTE J1650−500 was first detected by the All-Sky Monitor (ASM; Levine et al. 1996) on board the *Rossi X-ray Timing Explorer (RXTE)* in 2001 September (Remillard 2001). The optical and radio counterparts were identified by Castro-

Tirado et al. (2001) and Groot et al. (2001), respectively. Augusteijn, Coe & Groot (2001) suggest a long orbital period and a low-mass secondary. Pointed X-ray observations by *RXTE* show strong low frequency QPOs and band limited timing noise (Wijnands, Miller & Lewin 2001), while *Chandra* revealed ionized iron absorption lines (Miller et al. 2002b). The X-ray flux started to decay 45 days after the beginning of the outburst, and a transition to the hard state occurred. During the hard state, additional radio measurements were made and an inverted spectrum indicative of a compact jet was observed (S. Corbel, private communication). Around 10 days after the state transition, the source was unobservable due to the Sun. After the Sun gap, the X-ray flux showed a modulation with a $\sim$14 day period (Tomsick et al. 2002b). The mass function has yet to be measured, however both the X-ray spectra, and the temporal properties are similar to the known Galactic black hole candidates (BHC). Moreover, a recent *XMM-Newton* analysis of the broad iron line feature suggests that XTE J1650$-$500 is a rapidly rotating black hole (Miller et al. 2002a).

In this paper, we search for high frequency QPOs and study the evolution of the low frequency QPOs through the decay. We investigate the evolution of the continuum parameters of the power spectra during the transition, and compare the temporal properties to the previous observations and other BHCs. We also employ other temporal analysis tools related to the cross spectrum, namely the frequency dependent time lags and coherence function.

2. Observations and Analysis

We analyzed the PCA/*RXTE* (Proportional Counter Array, see Bradt, Rothschild & Swank (1993) for a description of *RXTE*) data from observations of XTE J1650$-$500 from the start of the decay ($\sim$MJD[9] 52218) until the source was close to the sun between MJD 52240 – 52266 (see Fig. 1). When it was observable again, the flux had decayed significantly. Until MJD 52230 the X-ray energy spectrum was typical of a HS black hole spectrum. Between MJD 52230 and 52232 (around the dashed line in Fig. 1) the energy spectrum hardened.[10] For the observation at MJD 52232, both the energy spectrum and the power spectrum showed significant changes and a transition to the hard state occurred. (The first square after the dashed line in Fig. 1.) We call this observation Obs 1, and number the following observations according to their date of observation. Before the transition, the variability was very weak and the power spectrum was not above the noise level. We obtained a PSD by

[9]Modified Julian Date (MJD = JD - 2400000.5)

[10]The detailed spectral analysis of XTE J1650$-$500 during the outburst decay from the *RXTE* and the *Chandra* observations will be presented in a separate paper by Tomsick et al. (2002a).

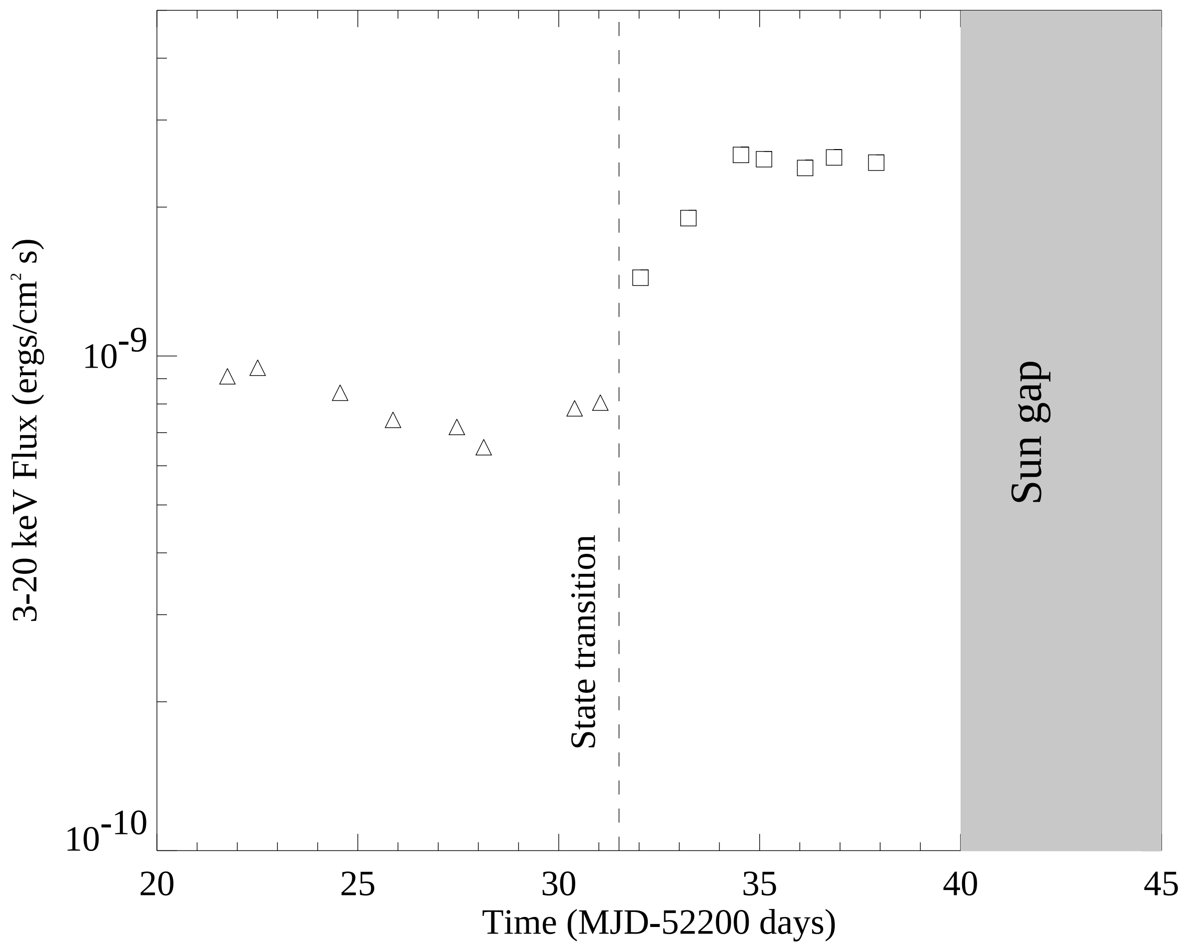

Fig. 1.— PCA light curve of XTE J1650−500 in 3 – 20 keV band. The dashed line represents the time when the state transition occurred. The observations represented by squares are the ones that we focus on in this paper. The gray area is the time when the source is close to the sun and unobservable. The 3 – 20 keV X-ray flux increases during the transition to the LS which is uncharacteristic for BHCs.

combining light curves from our 10 observations in the HS and fitted it with a Lorentzian, which resulted in a 95% confidence rms amplitude upper limit of 4%. The rms amplitude jumped to 17% for Obs 1, and a weak QPO at 8.71 Hz is observed for Obs 2. For the following observations until the sun gap, both the energy spectrum and the power spectrum showed characteristics of a typical hard state (see Fig. 2). In this paper, we focus on the 7 observations after the state transition and before the sun gap, represented by the squares in Fig. 1. Due to the drastic change in the flux and the low quality of the temporal data, the observations after the sun gap are not included in this work.

We used the standard *RXTE* data analysis software FTOOLS 5.1 to extract light curves. For all observations, the data were accumulated in an event mode with 125 μs time resolution and 64 energy channels. Typical integration times were 1 – 2 ks per observation. We used all of the Proportional Counter Units (PCU) that were on simultaneously for the timing analysis. The observations were made after the loss of the propane layer for PCU 0, and we dealt with the additional background as described in Kalemci et al. (2001). For each observation, we computed the power spectra and cross spectra using IDL programs developed at the University of Tübingen (Pottschmidt 2002) for three energy bands, 2 – 6 keV, 6 – 15 keV, and 15 – 30 keV and combined band of 2 – 30 keV. Above 30 keV, the source is not significantly above the background. The PSD was normalized as described in Miyamoto & Kitamoto (1989) and corrected for the dead time effects according to Zhang et al. (1995) with a dead-time of 10 μs per event. First, we searched for high frequency QPOs using short 1 second segments with a Nyquist frequency of 2048 Hz using the summed energy band of 2–30 keV. We did not detect any high frequency QPO in any of our observations. The 95% confidence upper limits on the rms amplitude for QPOs above 50 Hz with a fixed quality value of $Q = 6$ are between 3.7 – 4.4 % for different observations. Next, using 128 second time segments, we investigated the low frequency QPOs and the timing properties of the continuum up to 256 Hz. We also analyzed the time lags and coherence function between 2 – 6 keV and 6 – 15 keV energy band light curves.

3. Results

Historically, the PSD of BHCs during the low state has been modeled by a broken power law (or power laws with more than one break) plus narrow Lorentzians to fit the QPOs (Nowak et al. 1999; Tomsick & Kaaret 2000). This model is a good representation of our PSDs also. However, recent papers successfully fit several BHC and neutron star PSDs with broad Lorentzians for the continuum and narrow Lorentzians for the QPOs (van Straaten et al. 2001; Pottschmidt et al. 2002; Belloni, Psaltis & van der Klis 2002). When we fit our data with broad and narrow Lorentzians we see that this modeling represents the PSDs as well as or better than the broken power law in terms of χ^2 statistics. Although we did both kinds of fitting, we only present the Lorentzian fits. This allows for an easier comparison to recent work, for example on Cyg X-1 by Pottschmidt et al. (2002).

3.1. Lorentzian fits

We fit all our PSDs with Lorentzians of the form

$$L_i(f) \;=\; \frac{R_i^2\,\Delta_i}{2\,\pi\,[(f-f_i)^2+(\frac{1}{2}\,\Delta_i)^2]} \tag{1}$$

where subscript i denotes each Lorentzian component in the fit, R_i is the rms amplitude of the Lorentzian, Δ_i is the full-width-half-maximum, and f_i is the resonance frequency. A useful quantity of the Lorentzian is the frequency at which its contribution to the total rms variability is maximum (hereafter peak frequency):

$$\nu_i \;=\; f_i\,\left(\frac{\Delta_i^2}{4\,f_i^2}+1\right)^{1/2} \tag{2}$$

In Fig. 2, we plot the power spectra in the form of PSD $\times$ frequency and over-plot the Lorentzian fits. In this figure, the Lorentzians peak at ν_i not at f_i. In this section, including the tables, Lorentzian frequency means the peak frequency, not the resonance frequency. Most of our observations contain a Lorentzian that is narrow (with $Q > 2$, as compared to $Q < 1$ for broad Lorentzians) which we call a QPO. The QPO frequencies reported here are the resonance frequencies to make them easier to be compared to previous reports.

As seen in Fig. 2, except for the first observation, each observation requires at least two broad Lorentzians to fit the continuum, and a QPO (see Table 1 for the fit parameters). For Obs 1, the 95% confidence upper limit on the rms amplitude of a QPO in 0.1 - 20 Hz range with a Q = 6 is 2.8 %. The QPO is always the second peaked component in the PSD. Although the second peaked component in Obs 4 has a quality value of ~1.5, it is still quoted as a QPO for consistency. Since they are narrow, the quoted resonance frequencies are very close to the peak frequencies[11]. We call the broad Lorentzians in the fit L_i, where i=1 is the lowest frequency peak Lorentzian. The QPO is not counted and always referred as the QPO throughout the paper.

[11]The peak frequency and the resonance frequency differ by 5% for the worst case of Obs 4.

There is an overall shift to lower frequencies with time for both the wide Lorentzians and the QPOs (see Fig. 3a). The overall rms amplitude increases with time, and settles around 35% after Obs 5 as seen in Fig. 3b. The rms amplitudes of individual Lorentzian components do not show a regular trend and can be found in Table 1.

We also study the dependence of temporal properties on energy. We fit the PSDs from two energy band light curves, 2 – 6 keV and 6 – 15 keV, and study the evolution of the peak frequencies and the rms amplitudes of Lorentzian components. Fig. 4 summarizes our efforts, where we plot the peak frequencies and the rms amplitudes of L_1 in the two energy bands mentioned. For Obs 1, during the state transition, there is a clear shift with energy in the peak frequency of L_1, the only component in the PSD fit as seen in Fig. 5. The 6 – 15 keV L_1 peaks at 3.50 ± 0.42 Hz, whereas the 2 – 6 keV L_1 peaks at 9.70 ± 2.16 Hz. Moreover, the 6 – 15 keV rms amplitude is higher than the 2 – 6 keV amplitude. For the remaining observations, the 2 – 6 keV rms amplitude is higher, and the Lorentzians peak at the same frequency (within 1-σ error).

It was shown recently that ν_i is an important parameter in terms of frequency correlations (Nowak 2000; van Straaten et al. 2001; Pottschmidt et al. 2002). Having observed these correlations in other sources, we decided to look for them in XTE J1650$-$500, and plotted peak and QPO frequencies as a function of each other. Two sets of parameter correlations are apparent as shown in Fig. 6; ν_2 and ν_1 show a correlation similar to the one reported by Psaltis, Belloni & van der Klis (1999), and ν_1 shows a correlation with the QPO frequency which is shown to exist for other black hole and neutron star sources (Wijnands & van der Klis 1999). Due to low statistics and large errors, we could not conclude whether ν_3 correlates with ν_1.

3.2. Time lags and coherence

One can use the cross-spectral elements of the Fourier transform to obtain other information. The coherence function, for example, is a Fourier-frequency-dependent measure of the degree of linear correlation between two concurrent time series, in this case light curves measured simultaneously in two energy bands (Nowak et al. 1999). For example, unity coherence means that there exists a linear transformation function between two energy bands for each piece of light curve that we are averaging and this function is the same for every piece. The Fourier time lag is a Fourier-frequency-dependent measure of the time delay between two concurrent time series (Miyamoto & Kitamoto 1989; Nowak et al. 1999). It is related to the phase of the average cross power spectrum between the "soft energy" light curve and the "hard energy" light curve. We use the convention that the sign of the lag

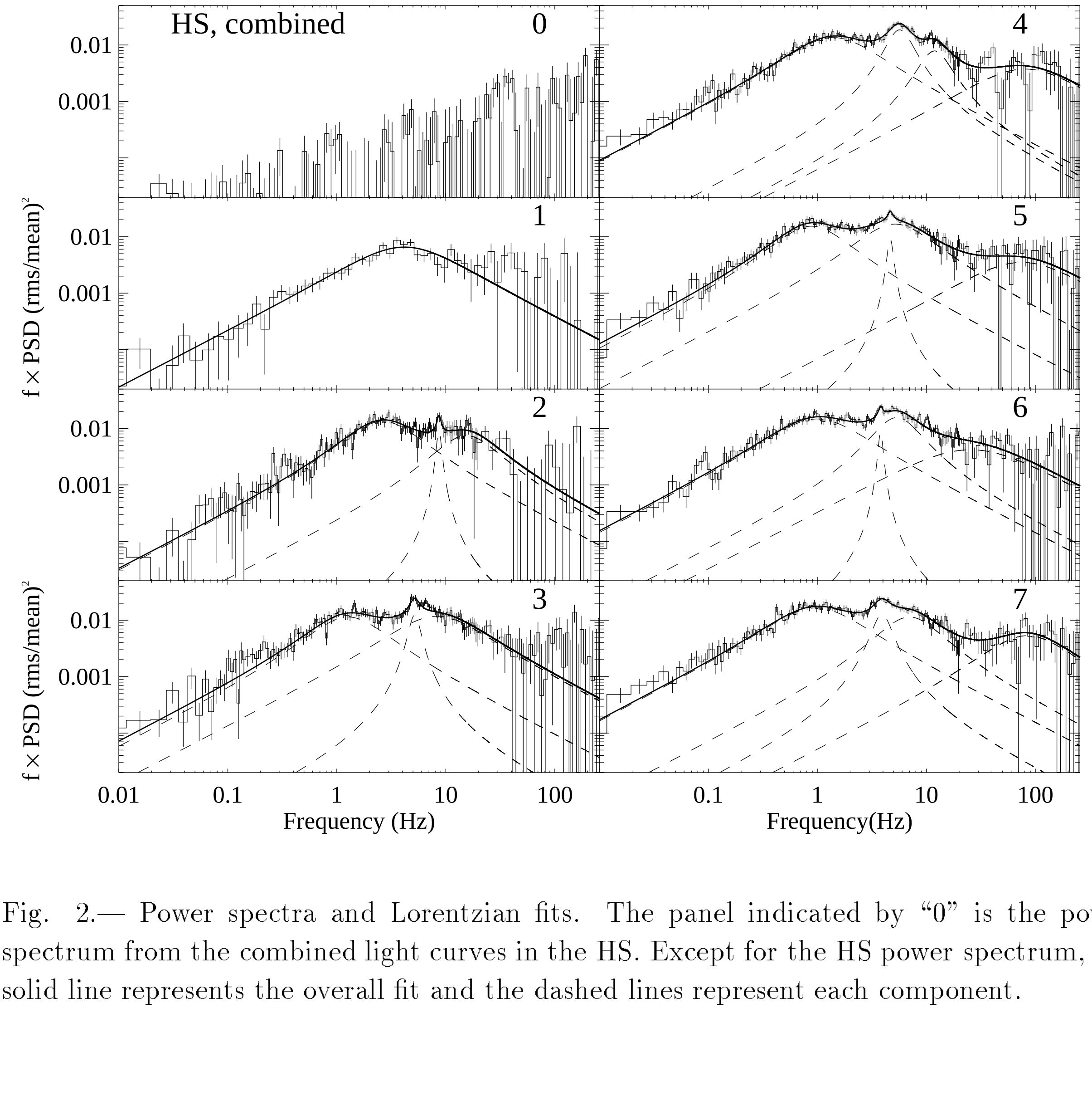

Fig. 2.— Power spectra and Lorentzian fits. The panel indicated by "0" is the power spectrum from the combined light curves in the HS. Except for the HS power spectrum, the solid line represents the overall fit and the dashed lines represent each component.

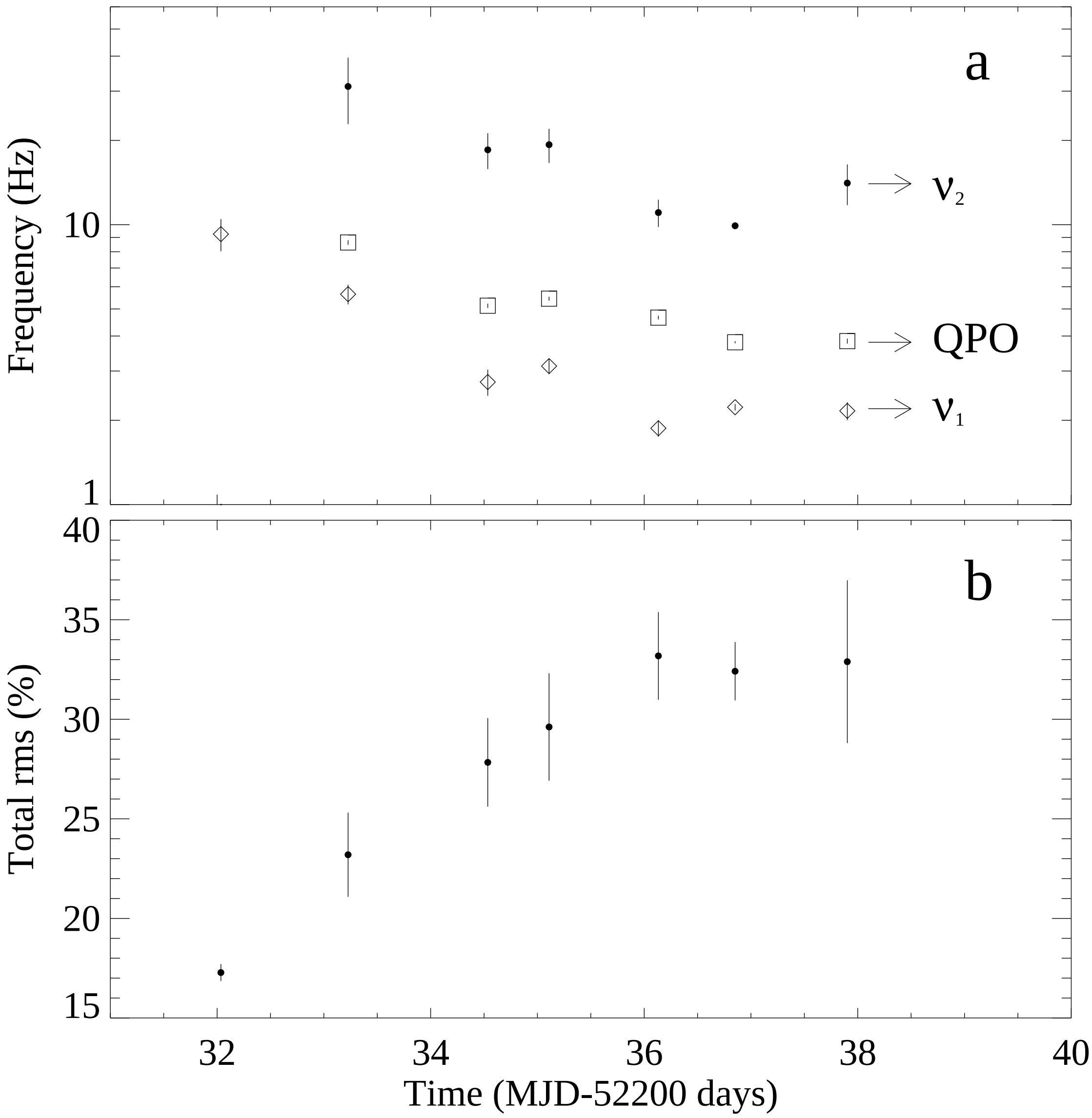

Fig. 3.— Lorentzian fit parameters: (a) Peak frequencies of the Lorentzians and the resonance frequencies of the QPOs. Filled circle represents ν_2, open square represents QPO frequency and diamond represents ν_1. (b) Total rms amplitude of the Lorentzians, including the QPO. During the HS, the total rms amplitude has 95% confidence upper limit of 4%.

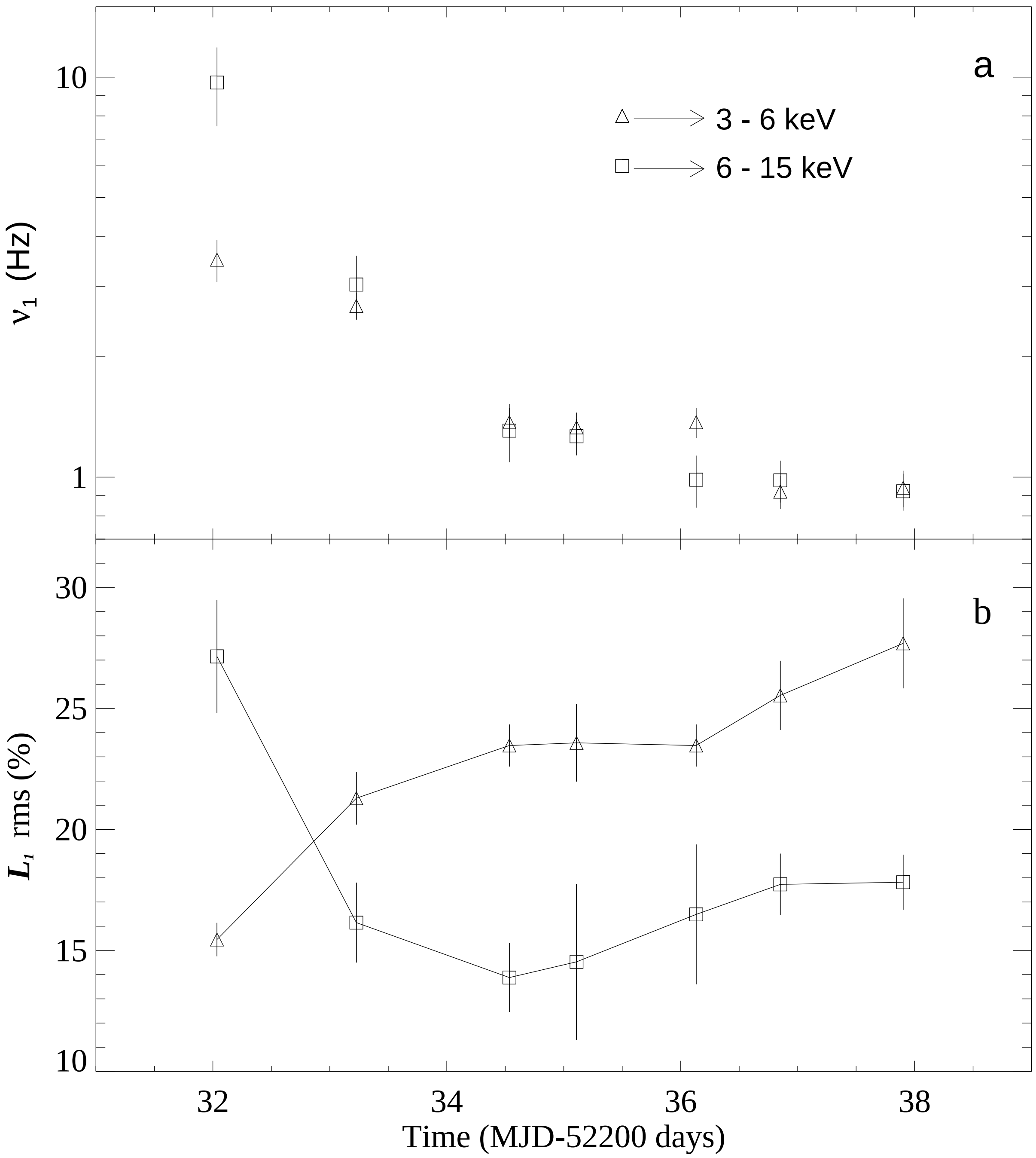

Fig. 4.— Energy dependence of PSD fit parameters: (a) Peak frequencies of L_1. Squares represent the 6 – 15 keV results, and triangles represent the 2 – 6 keV results. The 6 – 15 keV peak frequency for the first observation is clearly higher than the 2 – 6 keV one. For the remaining observations, the peak frequencies are the same for both energy bands within 1-σ error. (b) Rms amplitude in the two energy bands mentioned.

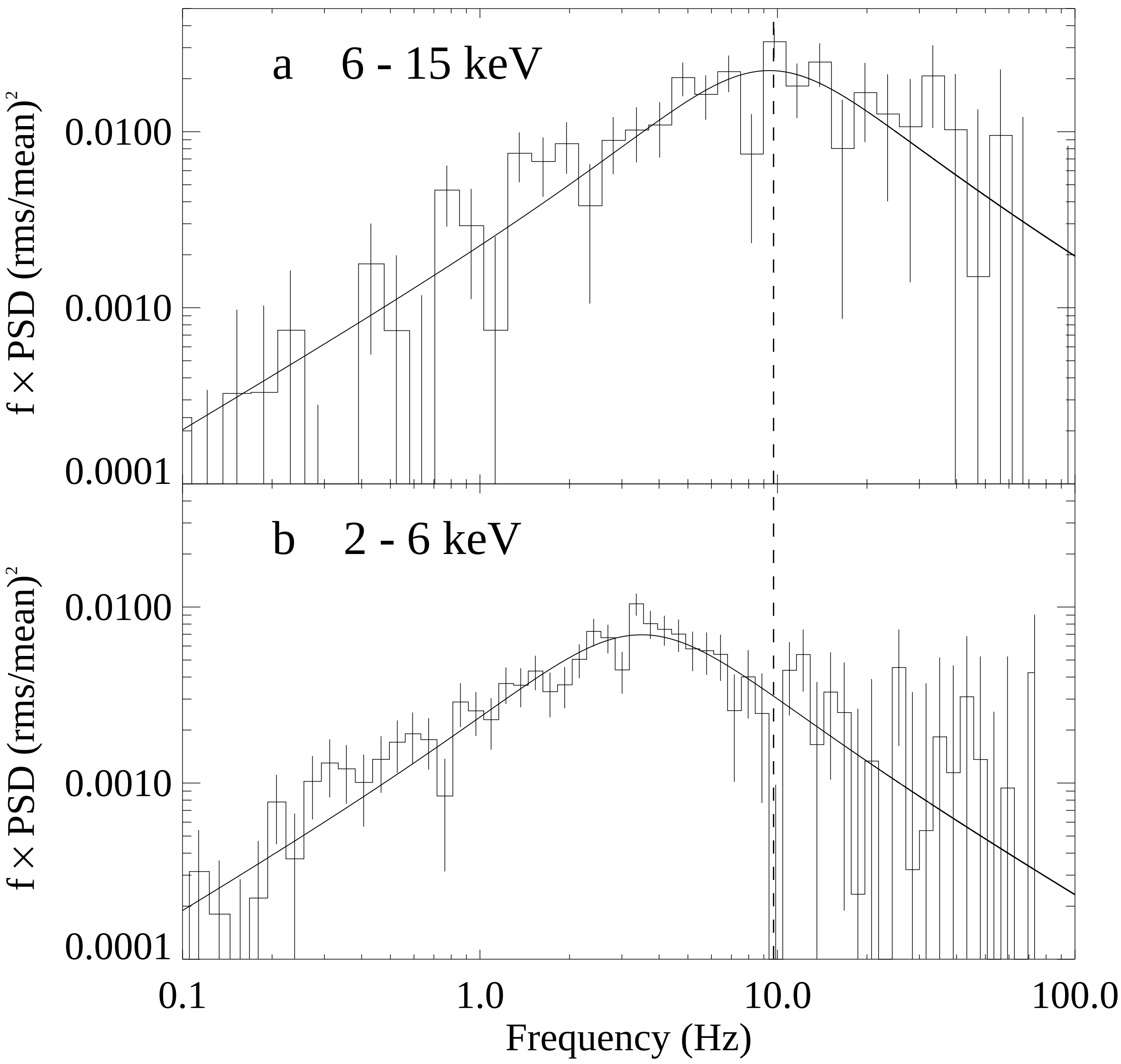

Fig. 5.— Fits to the power spectra of Obs 1 in two energy bands: (a) 6 – 15 keV, (b) 2 – 6 keV. As clearly seen, the 6 – 15 keV Lorentzian peaks at a higher frequency and has higher rms amplitude for this observation. The dashed line is the peak frequency of the Lorentzian in the 6 – 15 keV band.

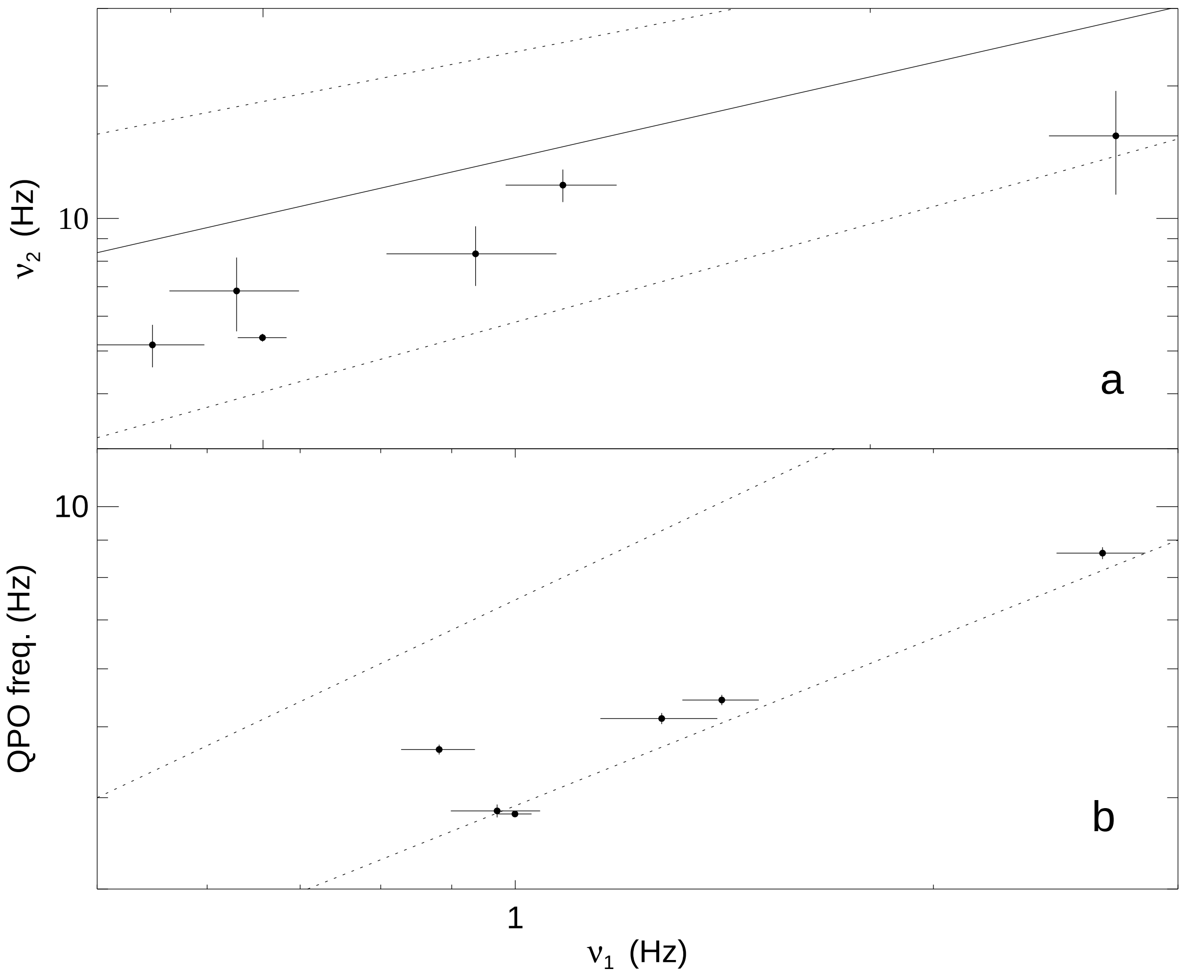

Fig. 6.— Frequency correlations: (a) Correlation between the peak frequencies of L_1 and L_2. The solid line is from Psaltis, Belloni & van der Klis (1999) which is their fit to the correlation between the narrow QPO frequency and the frequency of a peaked Lorentzian component that occurs at frequencies higher than the QPOs. The dashed lines are 1σ away from the solid line fit. (b) Correlation between ν_1 and the QPO frequency. The dotted lines represent the frequency range at which this correlation exists for other sources reported in Wijnands & van der Klis (1999).

is positive when hard photons lag soft photons. Observations of hard lags in BHCs have often been interpreted as evidence for Compton upscattering in a hot electron gas (Payne 1980), however simple Comptonization models have difficulty explaining the magnitude of lags (Ford et al. 1999).

Fig. 7 shows the evolution of mean coherence and mean time lag in 1 – 10 Hz where they are least affected by the Poisson noise. The mean lag decreases whereas the coherence function increases with time, and they both approach an asymptotic value. The time lag decays from 24 ms to around 6 ms, and the coherence increases from 0.6 to unity. Note that during the HS, the average coherence is consistent with being zero, therefore time lags have no physical meaning (Nowak et al. 1999). This is the third source after Cyg X-1 and GX 339−4 to show enhanced lags during the state transition. We also added the evolution of the hardness ratio of the X-ray spectrum to Fig. 7. The ratio is taken between the HEXTE Cluster A count rate in 17 – 150 keV band and the PCA count rate per PCU in 3 – 10 keV band. The hardness ratio is inversely related to the power-law index (Γ) of the X-ray spectrum, and preliminary spectral analysis confirms their anti-correlation. Γ and average lag have been shown to correlate for Cyg X-1 (Pottschmidt et al. 2002) and GX 339−4 (Nowak, Wilms & Dove 2002). The anti-correlation of the hardness ratio and the mean lag shows that XTE J1650−500 is similar to these sources.

4. Discussion

4.1. Comparison of XTE J1650−500 with other sources

The temporal properties of XTE J1650−500 during the transition to the hard state are very similar to what has been observed for other BHCs, namely 4U 1630−47 (Tomsick & Kaaret 2000), Cyg X-1 (Pottschmidt et al. 2002), and also XTE J1550−564 (Kalemci et al. 2001). For 4U 1630−47, a sharp transition was seen with most of the changes in the temporal properties occurring in less than 2 days during the decay of the 1998 outburst. Similarly, for XTE J1650−500, Obs 1 and our last HS observation are only one day apart. For 4U 1630−47 (during its 1998 decay) and for XTE J1550−564 (during its 2000 decay), the QPO frequency and the break frequency showed a decreasing trend, whereas the overall rms amplitude showed an increasing trend after the transition (Tomsick & Kaaret 2000; Kalemci et al. 2001), as observed in XTE J1650−500. On the other hand, the 3 – 20 keV X-ray flux decreased during and after the transition for these sources, whereas it increased during the transition for XTE J1650−500. This is likely due to the hardening of the power law index and the energy range of PCA. This behavior can be explained if we adapt the two parameter description of Homan et al. (2001) and assume that the second parameter is the size of the

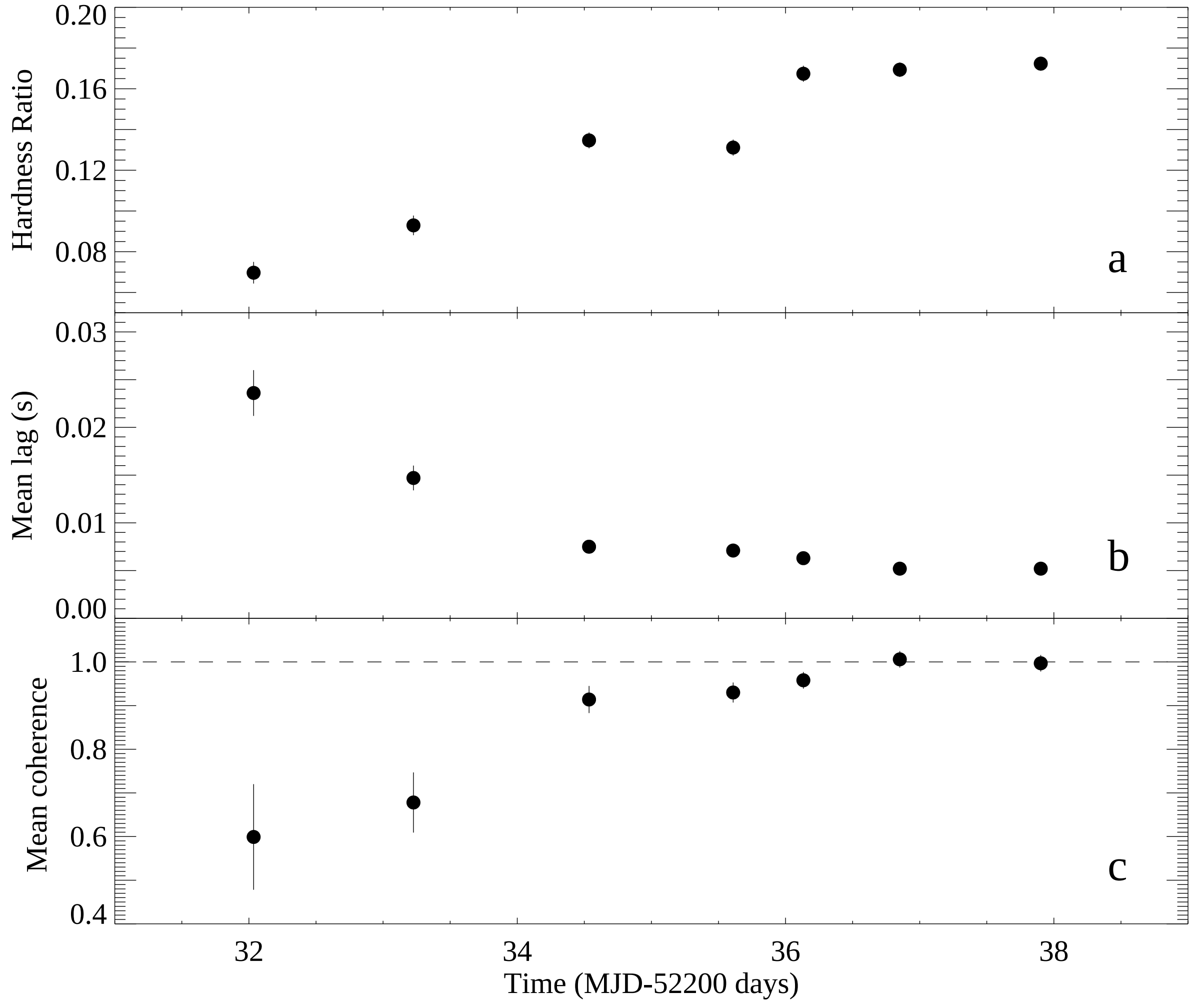

Fig. 7.— (a) Ratio of the HEXTE Cluster A count rate in 17 – 150 keV band to the PCA count rate per PCU in 3 – 10 keV band (hardness ratio), (b) mean lag and (c) mean coherence. The mean is taken in the frequency band of 1–10 Hz where the measurements are well above the noise level. The energy bands are 2–6 keV and 6–15 keV. For Obs 1 and 2, the lags are significantly longer compared to the following observations. The dashed line indicates the unity coherence. The anti-correlation between the mean time lag and the hardness ratio, as well as the anti-correlation between the lags and the coherence is clearly observed.

Comptonizing region. Then, the mass accretion rate through the disk may decrease, but the increasing size of the Comptonizing region may result in many hard photons in the PCA range which can increase the X-ray flux. We also note that there could be significant flux below 3 keV, and bolometric fluxes might be considerably higher, especially for the HS.

Finally, it seems that the changes observed in XTE J1650−500 during the transition to the hard state resemble best to the transitional episodes of Cyg X-1. First of all, the mean X-ray time lag in 1 – 10 Hz frequency range is longer and the mean coherence is low during the state transition as compared to later observations, just as in Cyg X-1 (Cui et al. 1997; Pottschmidt et al. 2002). The peak frequencies of L_1 and L_2 are significantly higher and L_3 is absent during the state transition, again very similar to what has been observed in Cyg X-1. Correlations between the peak frequencies of the Lorentzians, which we will discuss in Section 4.3, are also similar.

4.2. Lags and Coherence

During the transition, the average time lags are enhanced compared to the following observations as shown in Fig. 7. As mentioned earlier, this behavior has been seen before for Cyg X-1 and for GX 339−4 (Pottschmidt et al. 2000; Nowak, Wilms & Dove 2002). In Cyg X-1, the mean lags do not change during the LS and the soft state[12] and they have similar values, but they only increase during the failed state transitions. Pottschmidt et al. (2000) suggested that one possible reason is the optically thin radio outflows during the state transition which creates an additional Comptonizing area at its base that increases the time lags. It seems that the quenching of jets during the HS and the IS/VHS, optically thin outflows (and simultaneous building of a compact jet) during the state transitions, and optically thick emission during the LS are typical properties of BHCs (Corbel et al. 2000; Corbel et al. 2001; Fender 2001). For XTE J1650−500, there is no radio measurement during the state transition, but an inverted radio spectrum is observed during the hard state (S. Corbel, private communication), and it is likely that a large outflow occurred during the state transition as in other BHCs. Therefore, extended and hot material from optically thin ejections or from a compact jet building up could be the reason for the enhanced lags as hypothesized for Cyg X-1 and GX 339−4, and the reduced coherence could simply be a result of additional scatterings in the hot material. The spectral modeling of the corona and

[12]The soft state in Cyg X-1 is probably not the usual soft state as seen in other BHCs, but rather closer to the "very high state", and therefore direct comparisons with the HS of XTE J1650−500 and soft state of Cyg X-1 might not be correct.

the reflection features also seem to support this idea for Cyg X-1 and GX 339−4 (Nowak, Wilms & Dove 2002; Pottschmidt et al. 2002).

The reason for the lack of enhanced lags after Obs 2 could also be due to different Lorentzian components acting at the same frequency range. Nowak (2000) discussed the case that the overall measured time lag may be a composite of time lags inherent to each individual coherent PSD component. Although the individual time lags can be fairly large, the composite lag might be small. For Obs 1 the only apparent component present is L_1. Although we can not rule out the presence of a QPO, its rms upper limit amplitude is low compared to rms amplitude of L_1. For Obs 2, the 1 – 10 Hz band is dominated by L_1 (14% rms amplitude), where L_2 contributes little (2% rms amplitude). Moreover, the QPO, which is also within this frequency range, is weak. For the remaining observations, significant part of L_2 moves into this frequency range[13] and QPOs are strong (see Fig. 2). This could be the reason for the reduced time lags after Obs 11. Note that similar arguments have been raised to explain the enhanced lags in Cyg X-1 (Pottschmidt et al. 2002). One way to check this argument is to compare the frequency dependent lags with the shape of the power spectrum. Unfortunately, the quality of our time lag spectrum is not good enough to do this. However, the anti-correlation of the mean coherence with the mean lag seems to counter this argument since one would expect a decrease in the mean coherence in a frequency band where different processes are contributing. A steady state is reached after our third observation, and the time lags (correspondingly the phase lags) are small. For these cases, the Lorentzians could be due to individual coherent processes. One can still obtain near unity coherence if the phase lags are small as illustrated in Nowak, Wilms & Dove (1999), see especially equation (3) of this paper. In Fig. 7, we also included the evolution of the hardness ratio, since it anti-correlates with the mean time lag. Note that it also anti-correlates with the peak frequencies as in the case of Cyg X-1 and GX 339−4. The implications of this relation have been discussed extensively for GX 339−4 by Nowak, Wilms & Dove (2002).

4.3. Correlations between fit parameters

Various papers address the correlations between certain fit parameters of the PSD for X-ray binaries and show that these correlations exist for decades of frequency range (Wijnands & van der Klis 1999; Psaltis, Belloni & van der Klis 1999; van Straaten et al. 2001; Belloni, Psaltis & van der Klis 2002). One correlation is between the break frequency (nearly

---

[13]For example, for Obs 5, the relative rms contributions of L_1 and L_2 in 1 – 10 Hz range are 11% and 15%, respectively.

equivalent of ν_1) and the frequency of a "bump" or QPO above this break for different types of X-ray binaries: black hole candidates, atoll sources, millisecond X-ray pulsar and Z sources (Wijnands & van der Klis 1999). We obtained a box of frequency range from Fig. 2a of their paper which the correlation exists and over-plotted this to our QPO frequency versus ν_1 plot[14] in Fig. 6a. This plot shows that we can add XTE J1650−500 to the list of various other X-ray binaries for which this correlation holds.

There is another correlation reported by Psaltis, Belloni & van der Klis (1999) between the narrow QPO frequency and the frequency of a peaked Lorentzian component that occurs at frequencies higher than the QPOs. In our case this could be the QPO frequency vs ν_2 or QPO frequency vs ν_3. The former is not consistent with the correlation reported by Psaltis, Belloni & van der Klis (1999), and the latter is consistent within 1σ error bars, however the error bars on ν_3 are quiet large (see Table 1). The interesting result is that the correlation between ν_1 and ν_2 for XTE J1650−500 is consistent with the correlation reported by Psaltis, Belloni & van der Klis (1999) as shown in Fig. 6b. This is not very surprising since all these correlations have issues with the identification of the related components (Wijnands & van der Klis 1999; Psaltis, Belloni & van der Klis 1999; Belloni, Psaltis & van der Klis 2002). The same correlation between ν_1 and ν_2 is seen for Cyg X-1 also, adding one more to the similarities list.

4.4. Energy dependence of PSD components

Perhaps the most interesting result of this paper is the shifting of the peak frequency of L_1 to a higher frequency with increasing energy for Obs 1 as shown in Fig. 5. This kind of behavior has been seen with *Ginga* in two sources before, GX 339−4 and GS 1124−68 (Belloni et al. 1997). All those observations were in the VHS, except for one observation in GS 1124−68, where it was during the transition to the LS. This is the second time such a shift has been observed during a state transition. Belloni et al. (1997) interpreted the shifts as a result of shots with energy dependent amplitudes and profiles. We show in Fig. 4 that after Obs 1, there is no shift in the peak frequencies. This is hard to explain with the shot-noise models since it requires sudden removal of the energy dependence from the shot profile.

We attribute the frequency shift to a geometrical effect. We adapt the idea of the corona

[14]We also performed power-law fits and confirmed that the break frequency is close to ν_1. When we plot the break frequency - QPO frequency correlation from these fits, we obtained slightly better agreement with the Wijnands correlation.

being the part of a large vertically stretched conical outflow which explains enhanced lags and reduced coherence as discussed in Pottschmidt et al. (2002). One can add a temperature profile to the vertical scale such that the base of the outflow has a higher temperature. Then, the seed photons from the inner disk will interact predominantly with the higher temperature part of the jet at its base and will be scattered to higher energies. Assuming that the higher frequency variability in the accretion disk is created close to the inner edge, the high energy power spectrum would peak at higher frequencies. Similarly, seed photons originating away from the inner edge, which creates the low frequency variability, would interact predominantly with the cooler, higher altitude parts of the outflow. When the large outflow is over, the corona shrinks in the vertical scale which would cause a decrease in the X-ray lags and an increase in the coherence. Moreover, the temperature variation could be either absent or greatly reduced compared to the large outflow case which would also explain the disappearance of the frequency shift as observed for XTE J1650−500.

As mentioned earlier, the shift in the peak frequencies as a function of energy has been observed during the VHS and transitions. The radio emission is quenched in the IS/VHS, but a corona probably exists. Although this corona is probably not related to the "base of the jet" or an "optically thin outflow" as suggested in our model to explain XTE J1650−500 during the transition, the overall geometry in the IS/VHS might be similar, perhaps on a smaller scale. A systematic search on the frequency shift effect during the VHS for XTE J1650−500, and other sources during the IS/VHS and during the transitions can increase the number of constraints on the geometry of the accretion flow.

5. Summary and Conclusions

The similarities of temporal properties to those of other known black hole systems suggest that XTE J1650−500 is also a black hole system. Especially the similarities to Cyg X-1 are remarkable. Here is a summary of the temporal properties:

- The state transition is sharp in terms of the temporal properties with the appearance of band limited noise in the PSD. The rms amplitude increases from 4% upper limit in HS to $\sim$16% during Obs 1. The last HS observation and Obs 1 are only one day apart.
- The PSD can be characterized by broad Lorentzians and QPOs. The characteristic frequencies of these components decrease after the transition to the LS occurs, which can be interpreted as retreating of the inner disk radius as discussed in di Matteo & Psaltis (1999) for other BHCs. The total rms amplitude also increases during this time.

- The peak frequencies obey the correlations reported by Wijnands & van der Klis (1999) and Psaltis, Belloni & van der Klis (1999).
- The average lags are higher during the first two observations than the remaining observations. Likewise, the hardness ratio shows an increasing behavior as the transition occurs. The coherence function anti-correlates with mean lag and increase during the transition, and becomes unity coherence for the last two observations.
- L_1 peaks at different frequencies for different energy bands during Obs 1. After this observation this shift disappears. Also, the rms amplitude of L_1 increases with energy only for the first observation whereas it decreases with energy for the remaining observations. The shift can be a sign of temperature gradient at the base of the jet as discussed in Section 4.4.

EK acknowledges useful discussions with Jörn Wilms, Mike Nowak and Craig Markwardt. The authors would like to thank all scientists contributed to the Tübingen Timing Tools. EK was partially supported by TÜBİTAK. JAT acknowledges partial support from NASA grant NAG5-10886. KP was supported by grant Sta 173/25-1 and Sta 173/25-3 of the Deutsche Forschungsgemeinschaft. RW was supported by NASA through Chandra Postdoctoral Fellowship grant number PF9-10010 awarded by CXC, which is operated by SAO for NASA under contract NAS8-39073. PK acknowledges partial support from NASA grant NAG5-7405.

REFERENCES

Augusteijn, T., Coe, M., & Groot, P., 2001, IAU Circular, 7710

Belloni, T., Psaltis, P., & van der Klis, M., 2002, ApJ, submitted, astro-ph/0202213

Belloni, T., van der Klis, M., Lewin, W. H. G., van Paradijs, J., Dotani, T., Mitsuda, K., & Miyamoto, S., 1997, A&A, 322, 857

Bradt, H. V., Rothschild, R. E., & Swank, J. H., 1993, A&AS, 97, 355

Castro-Tirado, A. J., Kilmartin, P., Gilmore, A., Petterson, O., Bond, I., Yock, P., & Sanchez-Fernandez, C., 2001, IAU Circular, 7707

Corbel, S., Fender, R. P., Tzioumis, A. K., Nowak, M., McIntyre, V., Durouchoux, P., & Sood, R., 2000, A&A, 359, 251

Corbel, S., et al., 2001, ApJ, 554, 43

Cui, W., Zhang, S. N., Focke, W., & Swank, J. H., 1997, ApJ, 484, 383

di Matteo, T., & Psaltis, D., 1999, ApJ, 526, L101

Fender, R., et al., 1999, ApJ, 519, L165

Fender, R. P., 2001, MNRAS, 322, 31

Fender, R. P., Hjellming, R. M., Tilanus, R. P. J., Pooley, G. G., Deane, J. R., Ogley, R. N., & Spencer, R. E., 2001, MNRAS, 322, L23

Ford, E. C., van der Klis, M., Méndez, M., van Paradjs, J., & Kaaret, P., 1999, ApJ, 512, L31

Groot, P., Tingay, S., Udalski, A., & Miller, J., 2001, IAU Circular, 7708

Homan, J., Wijnands, R., van der Klis, M., Belloni, T., van Paradijs, J., Klein-Wolt, M., Fender, R., & Méndez, M., 2001, ApJS, 132, 377

Kalemci, E., Tomsick, J. A., Rothschild, R. E., Pottschmidt, K., & Kaaret, P., 2001, ApJ, 563, 239

Levine, A. M., Bradt, H., Cui, W., Jernigan, J. G., Morgan, E. H., Remillard, R., Shirey, R. E., & Smith, D. A., 1996, ApJ, 469, L33

Miller, J. M., Fabian, A. C., Wijnands, R., Reynolds, C. S., & Ehle, M., 2002a, ApJ, 570, 69

Miller, J. M., Wijnands, R., Wojdowski, P., Groot, P., Fabian, A. C., van der Klis, M., & Lewin, W., 2002b, The Astronomer's Telegram, #81

Miyamoto, S., & Kitamoto, S., 1989, Nature, 342, 773

Nowak, M. A., 2000, MNRAS, 318, 361

Nowak, M. A., Vaughan, B. A., Wilms, J. ., Dove, J. B., & Begelman, M. C., 1999, ApJ, 510, 874

Nowak, M. A., Wilms, J. ., & Dove, J. B., 1999, ApJ, 517, 355

Nowak, M. A., Wilms, J., & Dove, J. B., 2002, MNRAS, submitted, astro-ph/0201383

Payne, D., 1980, ApJ, 237, 951

Pottschmidt, K., 2002, PhD Thesis, Univ. of Tübingen

Pottschmidt, K., Wilms, J., Nowak, M. A., Heindl, W. A., Smith, D. M., & Staubert, R., 2000, A&A, 357, L17

Pottschmidt, K., et al., 2002, A&A, submitted, astro-ph/0202258

Psaltis, D., Belloni, T., & van der Klis, M., 1999, ApJ, 520, 262

Remillard, R., 2001, IAU Circular, 7707

Tanaka, Y., & Lewin, W. H. G., 1995, in X-ray Binaries, ed. W. H. G. Lewin, J. Van Paradjs, E. P. J. Van den Heuvel, (Cambridge: Cambridge U. Press), 126

Tomsick, J. A., et al., 2002a, in preperation

Tomsick, J. A., & Kaaret, P., 2000, ApJ, 537, 448

Tomsick, J. A., Kalemci, E., Corbel, S., & Kaaret, P., 2002b, IAU Circular, 7837

van Straaten, S., van der Klis, M., di Salvo, T., Belloni, T., & Psaltis, D., 2001, ApJ, in press, astro-ph/0107562

Wijnands, R., Miller, J. M., & Lewin, W. H. G., 2001, IAU Circular, 7715

Wijnands, R., & van der Klis, M., 1999, ApJ, 514, 939

Zhang, W., Jahoda, K., Swank, J. H., Morgan, E. H., & Giles, A. B., 1995, ApJ, 449, 930

This preprint was prepared with the AAS LaTeX macros v5.0.

Table 1: Lorentzian Fit Parameters (a)

Obs.	1	2	3	4	5	6	7
Date (MJD)[a]	52232.0	52233.2	52234.5	52235.1	52236.1	52236.9	52237.9
Flux[b]	2.60	2.75	2.68	2.56	2.30	2.29	2.15
Int. time[c]	1224	1488	1152	2000	1664	1824	1904
HR $\times 10^3$ [d]	70 ± 5	93 ± 5	135 ± 4	131 ± 4	167 ± 4	169 ± 4	172 ± 3
ν_1	4.18 ± 0.51	2.65 ± 0.19	1.28 ± 0.12	1.41 ± 0.09	0.88 ± 0.05	1.00 ± 0.03	0.97 ± 0.07
L_1 rms	17.28 ± 0.85	18.94 ± 0.90	17.72 ± 1.26	21.28 ± 0.56	18.71 ± 0.50	22.81 ± 0.20	24.00 ± 0.82
L_1 fwhm	7.96 ± 0.79	3.81 ± 0.37	1.88 ± 0.24	2.34 ± 0.15	1.18 ± 0.07	1.71 ± 0.04	1.65 ± 0.12
ν_2	-	15.41 ± 4.08	8.31 ± 1.29	11.91 ± 1.01	5.16 ± 0.57	4.68 ± 0.08	6.85 ± 1.30
L_2 rms	-	12.79 ± 2.27	20.26 ± 2.07	9.30 ± 1.44	26.21 ± 0.80	15.97 ± 1.94	16.38 ± 2.59
L_2 fwhm	-	19.06 ± 5.14	14.10 ± 1.41	8.11 ± 1.98	11.42 ± 0.71	5.23 ± 0.17	8.85 ± 1.07
ν_3	-	-	-	80.49 ± 40.71	85.70 ± 30.60	25.49 ± 2.77	84.99 ± 37.25
L_2 rms	-	-	-	12.87 ± 3.02	15.07 ± 1.40	16.17 ± 0.52	12.64 ± 2.68
L_3 fwhm	-	-	-	151.56 ± 58.87	171.41 ± 62.20	50.97 ± 5.50	131.67 ± 54.74
QPO freq.[e]	0.1-20[f]	8.64 ± 0.16	5.13 ± 0.09	5.44 ± 0.09	4.66 ± 0.07	3.80 ± 0.03	3.84 ± 0.08
QPO rms	<2.8[g]	3.98 ± 1.06	7.10 ± 1.12	13.12 ± 0.80	4.36 ± 0.94	3.72 ± 0.27	8.83 ± 2.09
QPO fwhm	$0.167 \times$ freq.[h]	0.98 ± 0.56	1.34 ± 0.39	3.29 ± 0.38	0.62 ± 0.27	0.39 ± 0.08	1.57 ± 0.48
χ^2/ν	56.0/67	144.1/144	153.6/144	166.8/152	125.5/141	182.7/141	137.6/141

[a] MJD at the beginning of the observation.

[b] Flux in 2–20 keV range, in units of $10^{-9}\,\mathrm{ergs\,cm^{-2}\,s^{-1}}$.

[c] Integration time in seconds.

[d] Ratio of the HEXTE Cluster A count rate in 17 – 150 keV band to the PCA count rate per PCU in 3 – 10 keV band, multiplied by 10^3.

[e] This is the resonance frequency, not the peak frequency

[f] Frequency range searched.

[g] 95% confidence upper limit.

[h] The width is fixed to $0.167 \times$ QPO frequency ($Q = 6$).